Dusty cloud properties and radiative forcing over dust source and downwind regions derived from A-Train data during the Pacific Dust Experiment

Wencai Wang,[1] Jianping Huang,[1] Patrick Minnis,[2] Yongxiang Hu,[2] Jiming Li,[1] Zhongwei Huang,[1] J. Kirk Ayers,[3] and Tianhe Wang[1,4]

Received 1 March 2010; revised 14 August 2010; accepted 25 August 2010; published 21 December 2010.

[1] Dusty cloud properties and radiative forcing over northwestern China (source region) are compared to the same quantities over the northwestern Pacific (downwind region) during the Pacific Dust Experiment (PACDEX; April 2007 to May 2007) using collocated data from three satellites in the A-Train constellation: CALIPSO (Cloud-Aerosol Lidar and Infrared Pathfinder Satellite Observations), the Clouds and Earth Radiant Energy System on Aqua, and CloudSat. Dusty clouds are defined as clouds extant in a dust plume environment (i.e., dust aerosols observed within 50 m of the cloud), while pure clouds are those in dust-free conditions. CALIPSO lidar and CloudSat radar measurements are used to discriminate between dusty and pure clouds in both study regions. It was found that dust aerosols change the microphysical characteristics of clouds, reducing the cloud optical depth, liquid and ice water path, and effective droplet size. The decreased cloud optical depths and water paths diminish the cloud cooling effect, leading to a greater warming effect. The dust aerosols cause an instantaneous net cloud cooling effect of 43.4% and 16.7% in the source and downwind regions, respectively. The dust aerosol effects appear to be greater for ice clouds than for liquid water clouds in the downwind region. These results are consistent with PACDEX aircraft observations.

Citation: Wang, W., J. Huang, P. Minnis, Y. Hu, J. Li, Z. Huang, J. K. Ayers, and T. Wang (2010), Dusty cloud properties and radiative forcing over dust source and downwind regions derived from A-Train data during the Pacific Dust Experiment, *J. Geophys. Res.*, *115*, D00H35, doi:10.1029/2010JD014109.

1. Introduction

[2] Asian dust storms can have significant impacts on the global climate system. These storms originate in the Taklimakan Desert of China and the Gobi Desert of Mongolia, most frequently in late winter and early spring. During an average year, sandstorms are observed on more than 20 days, while blowing sand occurs twice as often [*Zhou*, 2001]. *Li* [2004] estimates that the annual mean dust emission from China is about 800 kt. Besides contributing to regional and global climate change, dust aerosols affect the biosphere since they deposit minerals and soil in the ocean and on downwind land areas. They directly impact climate by scattering solar radiation and absorbing land-atmosphere long-wave (LW) radiation. Dust outbreaks also alter cloud droplet concentrations by increasing cloud condensation nucleus abundance and subsequently affecting the microphysical properties and cloud life cycle [*Niu*, 2001; *Huang et al.*, 2006a, 2006b]. Using a two-dimensional spectral-resolving cloud model, *Yin and Chen* [2007] simulated the effects of mineral dust particles on the development of cloud microphysics and precipitation over northern China. They showed that when dust particles are involved in cloud development as cloud condensation nuclei (CCN) and ice nuclei (IN) at the same time, the heating effect of dust aerosols and the increased dust aerosol loading will suppress precipitation because the enhancement of CCN is nearly overwhelmed by the stronger suppressing effect of IN [*Chen et al.*, 2007]. Furthermore, *Han et al.* [2008] found that the role of precipitation in suppressing dust storm occurrence is unimportant and that dust aerosols may play a more important role in suppressing the precipitation over arid and desert regions. This, in turn, could reduce the probability of precipitation, resulting in more complex and uncertain indirect effects.

[3] Clouds are another important factor in climate change; about 60% of the Earth's surface is covered with clouds [*Huang et al.*, 2006a]. On a global average basis, clouds cool the Earth-atmosphere system at the top of the atmo-

[1]Key Laboratory for Semi-Arid Climate Change of the Ministry of Education, College of Atmospheric Sciences, Lanzhou University, Lanzhou, P.R. China.
[2]NASA Langley Research Center, Hampton, Virginia, USA.
[3]Science Systems and Applications, Inc., Hampton, Virginia, USA.
[4]Also at Institute of Atmospheric Physics, Chinese Academy of Sciences, Beijing, P.R. China.

0148-0227/10/2010JD014109

sphere (TOA). Measurements from the Earth Radiation Budget Experiment [*Collins et al.*, 1994] indicate that small changes to cloud macrophysical (coverage, structure, altitude) and microphysical (droplet size, phase) properties have significant effects on climate. For instance, a 5% increase in short-wave (SW) cloud forcing would compensate for the increase in greenhouse gases that occurred during the period from 1750 through 2000 [*Ramaswamy et al.*, 2001].

[4] Owing to frequent sandstorms, sand and dust are always present in the atmosphere over dust source regions and form dust plumes in upper layers of the troposphere. These dust plumes often become entrained in westerlies, flow out from the continent to the open sea near Korea and Japan, and can impact the atmospheric hydrological and radiative budgets along the way [*Husar et al.*, 2001; *Zhang et al.*, 2003, *Huang et al.*, 2008]. The effect of this mixed dust-pollution plume on Pacific cloud systems and the associated radiative forcing (RF) constitutes an outstanding problem for understanding climate change and has not yet been explored [*Stith et al.*, 2009]. The primary reason that this problem has not been investigated is the lack of sufficient measurements of the plume's evolution as it crosses the Pacific Ocean. The international Pacific Dust Experiment (PACDEX) attempted to fill this observational gap by taking airborne measurements of dust and pollution transported from the western to the eastern Pacific and into North America. Under the framework of this campaign, intensive observations were carried out during April through May 2007 [*Stith et al.*, 2009] while the Afternoon or A-Train constellation of satellites was operational, providing valuable information about clouds and aerosols in the atmosphere at around 0130 or 1430 local solar time (LST) each day. Vertical profiles of clouds and aerosols were measured remotely by the Cloud-Aerosol Lidar and Infrared Pathfinder Satellite Observations (CALIPSO) lidar [*Winker et al.*, 2007] and the CloudSat radar [*Stephens et al.*, 2002]. Those narrow, near-nadir cross sections of the atmosphere are complemented by full-swath measurements of TOA broadband fluxes and retrievals of bulk cloud properties by the Clouds and the Earth's Radiant Energy System (CERES [see *Wielicki et al.*, 1998]) on the Aqua satellite.

[5] In this article we present a study of the dust effects on cloud and RF over two regions, the dust source region (northwestern China) and the downwind PACDEX region (northwestern Pacific and Sea of Japan; hereafter, the downwind region), during PACDEX (March 2007 to May 2007) using CALIPSO, CERES, and CloudSat measurements. Part of this study extends our previous research [*Huang et al.*, 2006a, 2006b] that examined dusty and dust-free clouds (hereafter, pure cloud) selected based on observations from surface meteorological stations in China and Mongolia. If no dust was observed at the surface, the overlying cloud observed by the satellite was defined as a pure cloud, but if the surface observation reported any dust event, the cloud was defined as a dusty cloud. This cloud selection procedure is not necessarily accurate because the dust and clouds could have occurred at different altitudes. CALIPSO and CloudSat, however, can observe aerosols and clouds at the same altitude [*Vaughan et al.*, 2004; *Hu et al.*, 2006, *Z. Liu et al.*, 2006, 2008; *Huang et al.*, 2007; *Winker et al.*, 2007], adding certainty that the dust can directly affect the clouds. In this study the CALIPSO lidar and CloudSat radar measurements are used to identify dusty and pure clouds in both dust source and downwind regions. Dusty clouds are defined as clouds that exist in a dust plume environment (i.e., dust aerosols observed within 50 m of the cloud in vertical or horizontal directions), while pure clouds are clouds having no dust aerosols within 500 m around them. The CALIPSO and CloudSat measurements, used in conjunction with the CERES data, should lead to a reliable analysis of the dust aerosol effect on cloud and RF over the PACDEX area and expand our understanding of their impact on the climate.

2. Data and Methods

[6] This study uses CALIPSO lidar level 2, Aqua CERES, and CloudSat observations taken between March and May 2007. All three satellites, part of the A-Train formation, are in Sun-synchronous orbits, with equatorial crossing times close to 0130 and 1430 LST. Since the orbital separation of these satellites is very small, they have closely matched temporal sampling and facilitate the merging of their respective datasets. CALIPSO acquires near-nadir vertical profiles of elastic backscatter at two wavelengths (532 and 1064 nm) during both day and night phases of the orbit. CALIPSO also provides profiles of linear depolarization at 532 nm, used to discriminate between ice and water clouds and to identify nonspherical aerosol particles. The primary products are three calibrated and geolocated lidar profiles: 532and 1064 nm attenuated backscatter and the 532 nm perpendicular polarization component. The depolarization ratio is computed directly from the ratio of two polarization components of the attenuated backscatter at 532 nm. The CALIPSO lidar level 2 data product (version 2.01) contains the cloud and aerosol layer reports along with the column properties. Level 1B data are first averaged to 5 km. The 5 km cloud layer products are used to screen out cloudy profiles [*Z. Liu et al.*, 2008].

[7] The CERES Single Scanner Footprint data used here combine CERES radiation measurements, imager-based cloud microphysical retrievals, and ancillary meteorology and aerosol fields to form a comprehensive, high-quality compilation of satellite-derived cloud, aerosol, and radiation budget information for radiation and climate studies. The Single Scanner Footprint instantaneous measurements include radiances, radiative fluxes at the surface and the top of the atmosphere, and a variety of parameters describing the clear and cloudy portions of the footprint [*Wielicki et al.*, 1996]. The CERES scanning broadband radiometers measure broadband SW (0.2–5.0 μm) and total radiances that are used to determine the TOA SW and LW (5–100 μm) fluxes using anisotropic correction models [*Loeb et al.*, 2005] that depend on the surface and cloud properties within the radiometer field of view. The scene types within each CERES scanner footprint are determined by analyzing collocated, high-resolution imager data. The Moderate Resolution Imaging Spectroradiometer (MODIS) provides the 1 km data for the cloud analysis. Cloudy pixels are identified over nonpolar regions using the method of *Minnis et al.* [2008a]. The Visible Infrared Solar-Infrared Split-Window Technique (VISST), described in detail by P. Minnis et al.

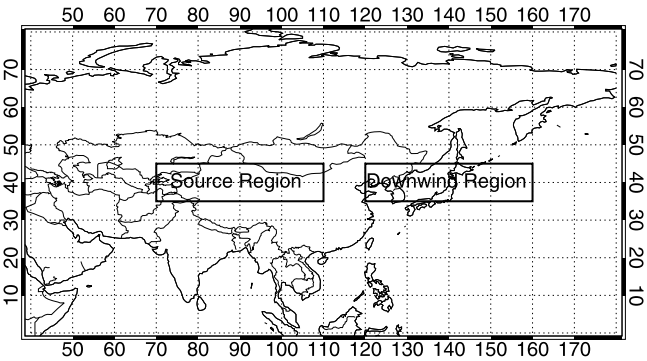

Figure 1. Regions selected to compare dust aerosol effect on cloud properties and cloud radiative forcing.

(CERES Edition-2 cloud property retrievals using TRMM VIRS and Terra and Aqua MODIS data, Part I: Algorithms, submitted to *IEEE Transactions on Geoscience and Remote Sensing*, 2010)], was used to derive daytime cloud properties. The VISST relies on 10.8 μm radiance to determine the effective temperature (T_e), 0.65 μm reflectance to obtain the cloud optical depth (OPD), 3.8 μm radiance to estimate the droplet effective radius (R_e), and the 12.0 μm channel to aid determination of the cloud phase. The cloud liquid water path (LWP) and ice water path (IWP) are then calculated from the retrieved cloud OPD and effective particle size, either the droplet R_e or the ice crystal effective diameter (D_e). T_e is used to determine the cloud effective radiating height (Z_e).

[8] A Single Scanner Footprint, defined for each CERES scanner footprint or field of view (field of view, 20 km resolution), consists of imager cloud retrievals, imager-based aerosol properties, and ancillary data merged with the broadband fluxes. All of the high-resolution data are convolved to match the point-spread function of the CERES scanner field of view. The cloud T_e corresponds to some location, the cloud Z_e, between the cloud base and the cloud top, typically within a hundred meters of the cloud top for liquid clouds and from a few hundred to several thousand meters below the cloud top for ice clouds. The corresponding depth in the cloud depends on the vertical distribution of cloud ice or liquid water content. Of the roughly 160 parameters in the Single Scanner Footprint data set, the current analysis uses the following: TOA SW and LW fluxes, cloud IWP or LWP, mean cloud T_e, mean cloud Z_e, R_e or D_e, and OPD.

[9] The instantaneous uncertainties in the CERES SW and LW TOA fluxes are 5%–10% and less than 3%, respectively [*Loeb et al.*, 2007]. The CERES cloud detection algorithm generally underestimates cloud cover. Clouds that are missed are typically small cumulus clouds that do not fill the imager pixel fields of view or very thin ice clouds that have an OPD < 0.3 [*Chiriaco et al.*, 2007; *Minnis et al.*, 2008a]. Such clouds are not an issue in this article. *Dong et al.* [2008] found that the means and standard deviations of the differences between the daytime CERES Aqua MODIS and the surface retrievals of R_e, OPD, and LWP for single-layered stratus are 0.2 ± 1.9 μm (2.5 ± 23.4%), 2.5 ± 7.8 (7.8 ± 24.3%), and 28.1 ± 52.7 g m^{-2} (17.2 ± 32.2%), from a total of 21 cases. The numbers in parentheses denote the percentage means and standard deviations. On average, the MODIS-derived cloud T_e values are 2.7 ± 2.4 K less than the surface-observed single-layered cloud center temperatures, with very high correlations (0.86–0.97). The VISST-retrieved stratus cloud Z_e values over land were found to be 0.5 ± 0.5 km lower than those observed by the surface lidars.

[10] Cirrus cloud (OPD < 3) Z_e values were found to be ~2.5 km below the cloud tops [*Mace et al.*, 2005], while the physical cloud top heights estimated by the VISST are often too low by 1.9 ± 2.2 km [*Smith et al.*, 2008]. The cloud-top height errors decrease with increasing OPD. *Mace et al.* [2005] and *Chiriaco et al.* [2007] found that mean values of D_e, OPD, and IWP retrieved by the VISST for cirrus clouds typically differ by 15 ± 30% from the same quantities derived from other instruments. While direct comparisons have not been performed for ice clouds with large OPDs, the average CERES Aqua MODIS retrievals of IWP are very similar in magnitude and distribution to those derived from CloudSat [*Waliser et al.*, 2009]. The uncertainties in the various parameters vary under different conditions and require many different validation studies for a full assessment. The parameter uncertainties determined so far, however, indicate that the CERES cloud properties are accurate enough for many studies.

[11] Humidity fields are taken from the reanalysis product of the National Centers for Environmental Prediction (NCEP). The NCEP/NCAR (National Center for Atmospheric Research) reanalysis project uses a state-of-the-art global numerical weather analysis and forecast system to perform data assimilation using historical observations, spanning the time period from 1957 to the present [*Kalnay et al.*, 1996]. The model used in the NCEP reanalysis has 28 vertical levels extending from the surface to 40 km, with a vertical resolution of 2 km near the tropical tropopause [*William et al.*, 2000]. These NCEP Final Operational Global Analysis data are provided on a 1° × 1° grid every 6 h. This product is from the Global Forecast System, which is run operationally four times a day in near-real time at the NCEP. Analyses are available for the surface, 26 mandatory (and other pressure) levels from 1000 to 10 mb, the surface boundary layer, some σ layers, the tropopause, and a few others. Parameters include surface pressure, sea level pressure, geopotential height, temperature, sea surface temperature, soil values, ice cover, relative humidity, u and v winds, vertical motion, vorticity, and ozone.

3. Dusty Cloud Identification

[12] Dusty clouds are defined as clouds that exist in a dust plume environment (i.e., dust aerosols observed within 50 m of the cloud). CALIPSO level 2 data are used as the primary cloud identification tool, with confirmation by CloudSat cloud mask data, which are from the 2B-GEOPROF products restricted to a cloud confidence ≥20 [*Mace et al.*, 2007]. The CALIPSO level 2 analysis identifies layers of enhanced backscatter as either aerosols or clouds. Here we define the clouds as dusty clouds if the aerosol and cloud layers are at the same height, or if the height difference (such as the height difference between the base height for the cloud layer and the top height for the aerosol layer) between them is within 50 m in the same areas, and the

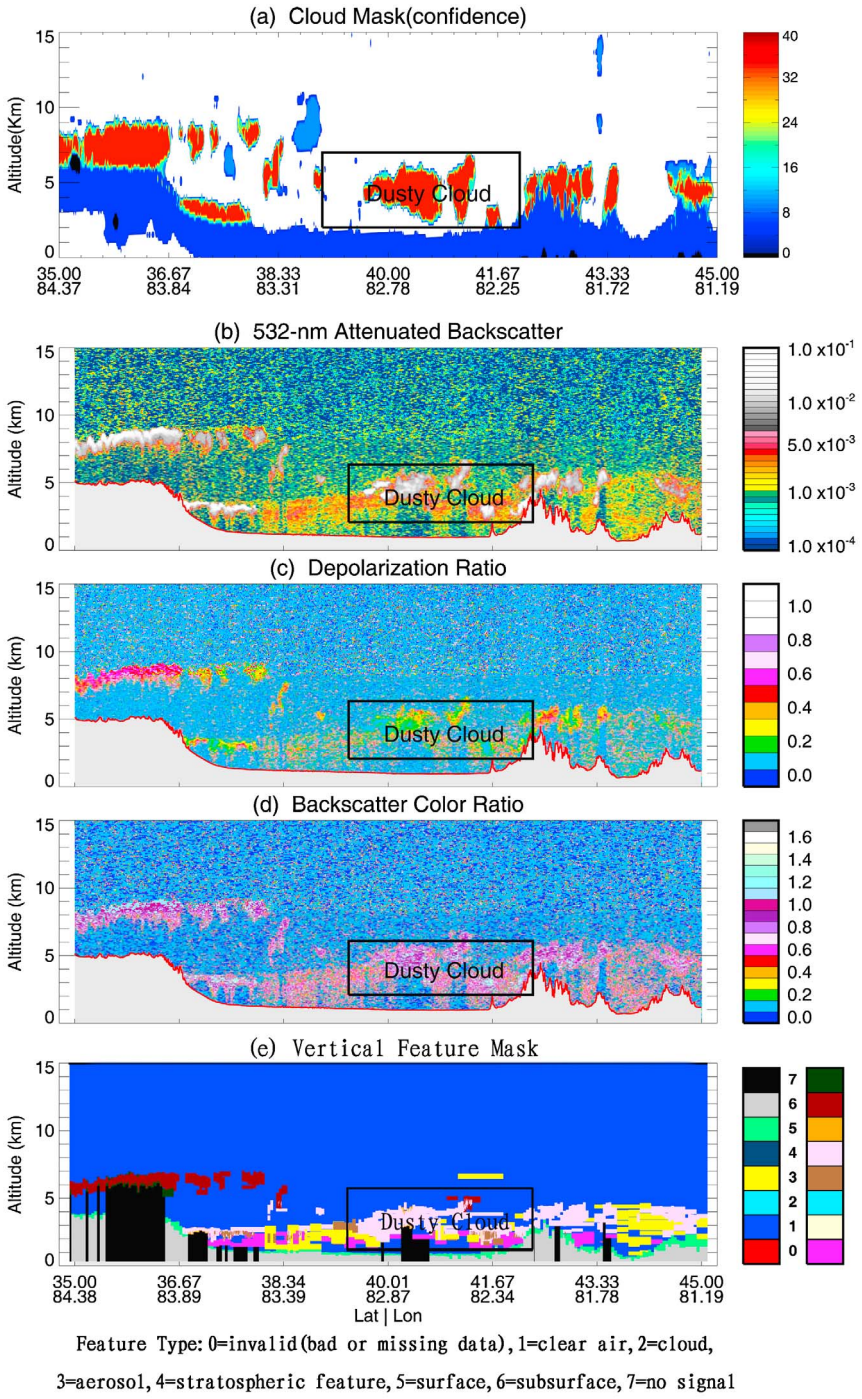

Figure 2. Vertical profiles of dusty cloud parameters in the source region, 5 March 2007. (a) CloudSat cloud mask image; (b) Cloud-Aerosol Lidar and Infrared Pathfinder Satellite Observations (CALIPSO) 532 nm total backscatter; (c) volume depolarization ratio; (d) 1064/532 nm backscatter color ratio; (e) vertical feature mask. The right color bar in Figure 2e indicates the type of clouds: 0, low overcast (transparent); 1, low overcast (opaque); 2, transition stratocumulus; 3, low, broken cumulus; 4, altocumulus (transparent); 5, altostratus (opaque); 6, cirrus (transparent); 7, deep convective (opaque).

aerosols are dust aerosols. The CALIPSO lidar level 2 vertical feature mask product, which describes the vertical and horizontal distribution of cloud and aerosol layers, is used to distinguish dust from other types of aerosols. In addition, identification of dust aerosols in a given altitude range of a lidar profile is accomplished by checking the volume depolarization ratio. The depolarization ratio of dust is high, owing to the nonspherical shape of the dust particles. For other types of aerosols the depolarization ratio is low (close to 0). Therefore, the depolarization ratio is used

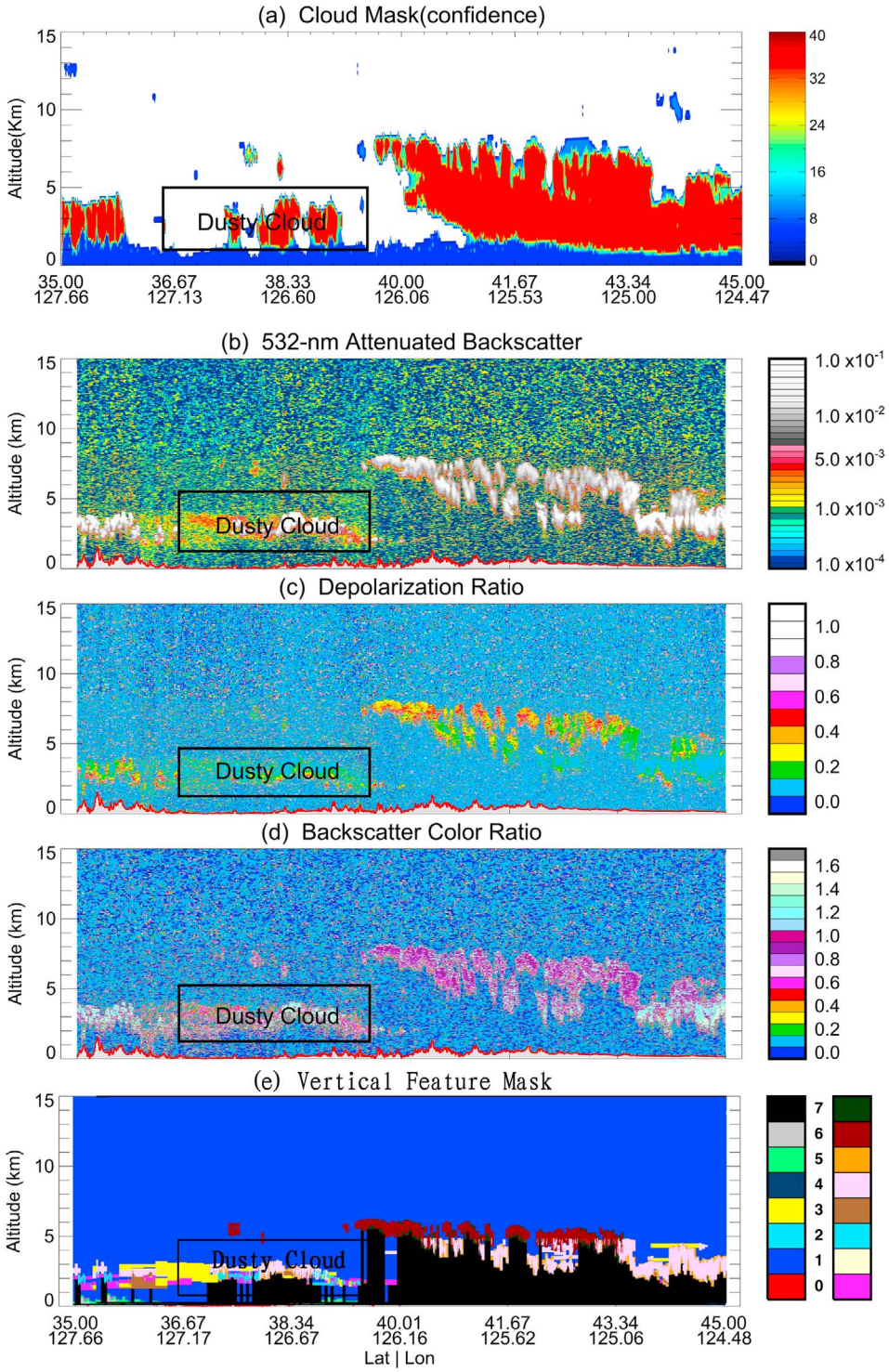

Figure 3. Same as Figure 2, but for 18 April 2007 in the downwind region.

as an indicator to separate dust from other aerosol types [*Murayama et al.*, 2001]. A threshold of 0.06 is used to detect the dust layer. *D. Liu et al.* [2008] provide a detailed description of CALIPSO data processing.

[13] To examine cloud modification induced by dust aerosols, the dust source and downwind regions were selected to investigate clouds in different regions. The dust source region extends from 35°N to 45°N and 70°E to

Table 1. Selected Source and Downwind Region Dust Cloud Cases in 2007

	Source Region				Downwind Region			
Case	Date Day	UTC Time	Latitude (deg)	Longitude (deg)	Date Day	UTC Time	Latitude (deg)	Longitude (deg)
1	5 Mar	7:44	38.08–39.19	83.13–83.47	21 Mar	4:26	35.67–36.60	133.36–133.64
2	19 Mar	6:17	35.04–37.36	105.33–106.01	22 Mar	5:10	37.47–40.98	121.20–122.30
3	21 Mar	7:45	39.20–41.51	82.41–83.14	23 Mar	4:14	36.34–39.50	135.58–136.54
4	21 Mar	7:46	42.98–44.35	81.44–81.92	31 Mar	4:29	41.67–44.67	121.5–122.52
5	2 Apr	8:09	37.50–40.17	76.66–77.48	1 Apr	4:09	41.32–42.16	136.27–136.54
6	4 Apr	7:58	41.52–44.23	78.40–79.31	2 Apr	4:51	36.51–38.83	126.52–127.21
7	10 Apr	7:20	38.34–41.76	88.51–89.59	7 Apr	5:09	35.23–37.33	122.34–122.95
8	12 Apr	7:08	39.54–43.00	91.18–92.31	7 Apr	5:11	41.64–43.73	120.28–120.99
9	20 Apr	7:57	38.49–41.12	79.46–80.28	8 Apr	4:15	39.66–43.22	134.36–135.53
10	21 Apr	7:02	40.31–42.58	92.88–93.62	8 Apr	4:16	43.26–44.90	133.77–134.35
11	22 Apr	7:45	39.85–42.16	82.21–82.96	10 Apr	4:02	37.39–40.90	138.23–139.32
12	1 May	7:38	37.21–39.97	84.46–85.31	11 Apr	4:45	36.46–39.71	127.79–128.77
13	6 May	6:19	41.40–44.24	103.12–104.09	11 Apr	4:46	41.18–43.58	126.52–127.32
14	6 May	7:57	38.04–41.51	79.33–80.42	18 Apr	4:51	36.1–39.35	126.36–127.34
15	14 May	7:07	36.68–39.48	92.34–93.19	4 May	4:51	35.94–39.41	126. 35–127.39
16	17 May	7:38	37.40–39.49	84.63–85.27	5 May	3:56	38.40–40.98	139. 76–140.57
17	20 May	7:39	37.67–40.0	76.64–77.40	11 May	3:18	35.16–36.01	150.55–150.79
18	22 May	6:18	39.17–41.04	104.21–104.80	14 May	3:50	39.78–42.22	140.89–141.69
19	22 May	7:57	38.13–39.15	80.09–80.40	20 May	4:51	35.81–38.35	126. 69–127.44
20	26 May	7:33	40.60–43.95	84.69–85.81	30 May	3:50	40.54–41.92	140.99–141.44

110°E, and the downwind region is bound by 35°N and 45°N and 120°E and 160°E (Figure 1). Figure 2 shows a typical dusty cloud observation, taken on 5 March 2007, in the source region. The red areas in Figure 2a are identified by CloudSat as clouds, but with very low confidence. Figures 2b, 2c, 2d and 2e, respectively, show plots of CALIPSO attenuated backscatter at 532 nm, volume depolarization ratio, backscatter color ratio (defined as the ratio of 1064 nm to 532 nm attenuated backscatter), and vertical feature mask. Dust aerosols have high volume depolarization ratio values and color ratios, owing to their nonsphericity and relatively large particle sizes, respectively. Other types of aerosols typically have low volume depolarization ratio values [*D. Liu et al.*, 2008; *Z. Liu et al.*, 2008]. For pollution aerosols, extinction is greater at 532 nm than at 1064 nm [*Huang et al.*, 2008]. From vertical feature mask information, we can see that cloud and dust aerosols are both present in this area. The values of the four parameters plotted in Figures 2b–2e indicate the presence of dust aerosols, and the cloud mask in Figures 2a and 2e denote

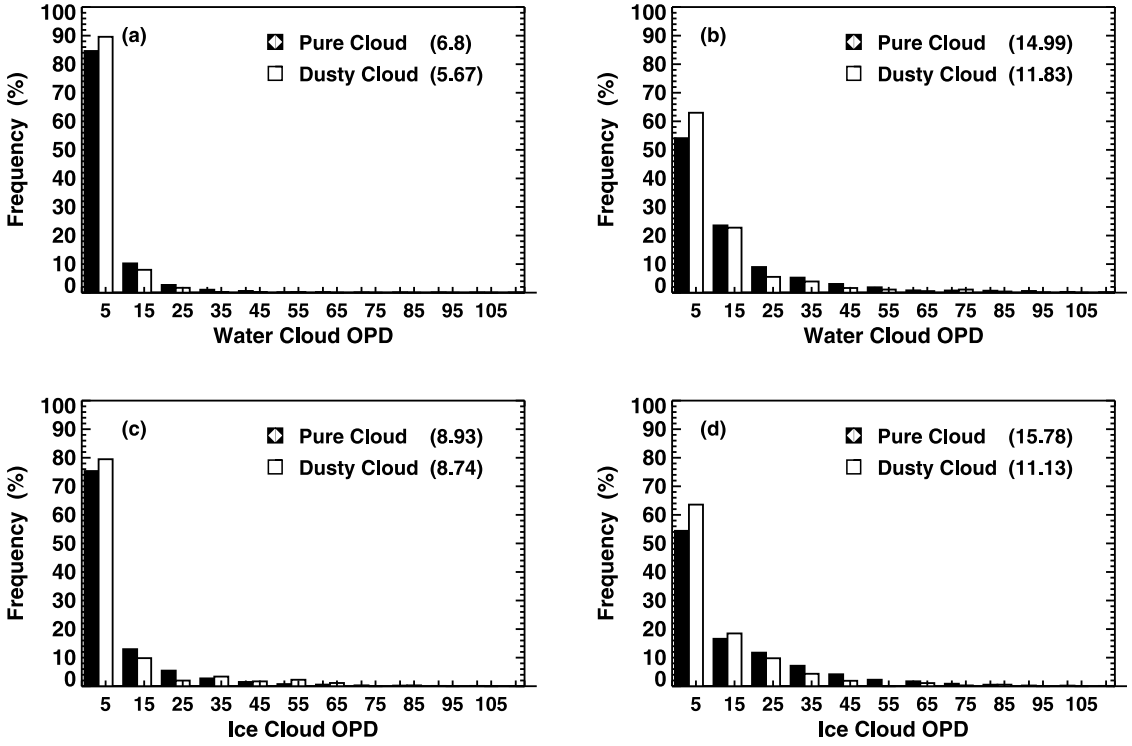

Figure 4. Comparison of (a, b) water cloud and (c, d) ice cloud optical depths (OPDs) between (a, c) the source and (b, d) downwind regions.

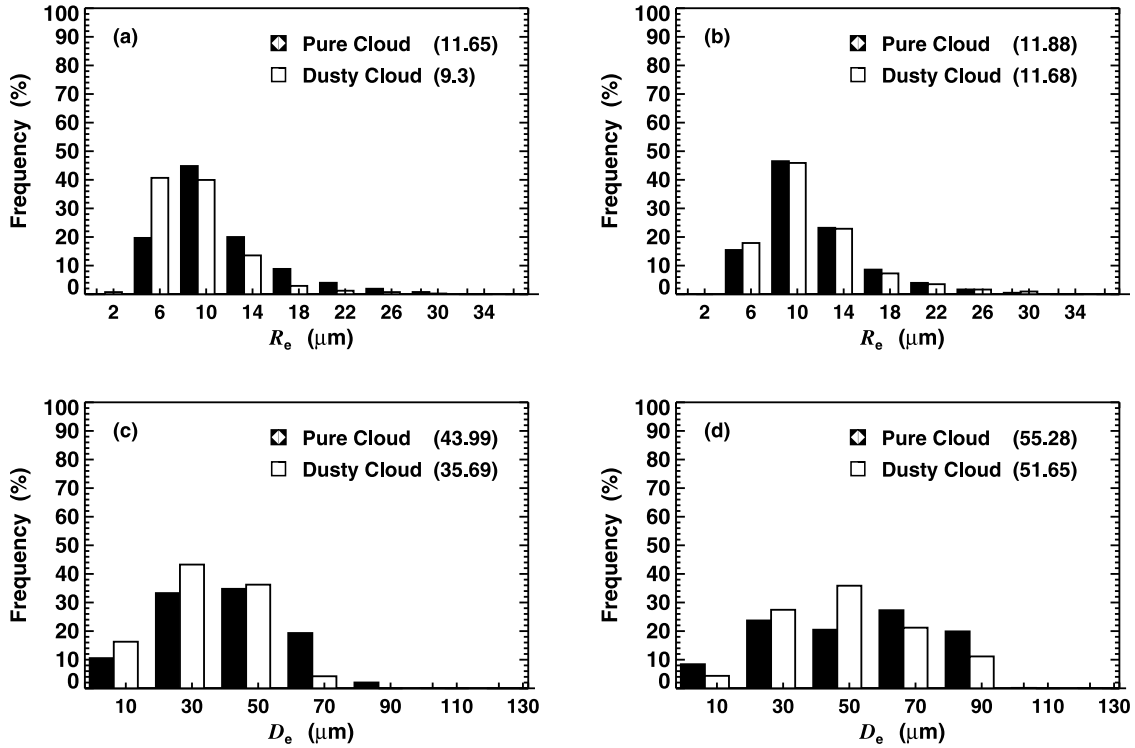

Figure 5. Same as Figure 4, but for water droplet effective radius (R_e) and ice particle effective diameter (D_e). Histogram intervals are 4 μm for droplet R_e and 20 μm for particle D_e.

the presence of cloud. CALIPSO data indicate that the aerosols are mostly dust. Using the information from all five plots in Figure 2, we define the cloud as a dusty cloud, which is denoted by the black rectangle.

[14] A similar observation from 18 April 2007, shown in Figure 3, shows a dusty cloud in the downwind region. CALIPSO data (Figures 3b–3e) show that the feature identified as a low-confidence cloud by CloudSat (Figure 3a) has dust aerosols in the same layers next to and below it. Figures 2 and 3 illustrate that dusty clouds exist in both the source and the downwind regions. Table 1 lists the 20 dusty cloud cases selected for each region.

4. Results

4.1. Cloud Properties

[15] To determine the differences in the properties between dusty and pure clouds, we also randomly selected 20 pure cloud cases each in the source and downwind regions during the period from March to May 2007. The sole criterion for selecting pure clouds is that the mean top and base pressures of the dusty and pure clouds are about equal, within ±1 km, according to the CALIPSO and Cloudsat data. This should minimize the effects of cloud type, cloud height, and other factors. So any differences between pure clouds and dusty clouds here are not likely owing to chance. For the water cloud cases the average cloud fractions for pure and dusty clouds are 59.0% and 46.6% in the source region and 80.9% and 69.4% in the downwind region, respectively. For the ice cloud cases the average cloud fractions for pure and dusty clouds are 68.8% and 47.3% in the source region and 91.2% and 73.3% in the downwind region, respectively.

[16] Histograms of the liquid water and ice cloud properties for each category from the 40 cases listed in Table 1 are shown in Figures 4 through 6 to compare the dusty and pure cloud properties, OPD, effective particle size, LWP, and IWP. Figure 4 shows the frequency distributions of dusty and pure cloud OPDs in the source and downwind regions. For water clouds in the source (Figure 4a) and downwind (Figure 4b) regions, the respective mean OPDs for pure clouds are 6.8 and 15.0, values that are 16.6% and 21.1% higher than those for the dusty clouds. For pure ice clouds (Figure 4c) the mean OPD is 8.9, which is negligibly higher than that for dusty ice clouds in the source region. In the downwind region (Figure 4d) the mean OPD for pure clouds is 15.8, 29.5% higher than the dusty cloud OPD. In addition, smaller OPD values occur more frequently for dusty clouds in both the source and the downwind regions.

[17] The frequency distributions of water droplet radius and ice particle diameter for pure and dusty clouds are shown in Figure 5. The mean R_e for pure clouds in the source region (Figure 5a) is 11.7 μm, compared to 9.3 μm for dusty clouds. In the downwind region (Figure 5b), however, the R_e means for pure clouds are much the same, differing by only 1.6%. The mean R_e for pure clouds is approximately the same for both source and downwind areas, but the average R_e for dusty clouds in the source region is smaller than that in the downwind region. As shown in Figure 5c, the mean D_e for pure ice clouds is 44.0 μm in the source region, while the dusty cloud mean is 35.7 μm, a decrease of 18.9%. In the downwind region (Figure 5d) the mean D_e for pure clouds is 55.3 μm,

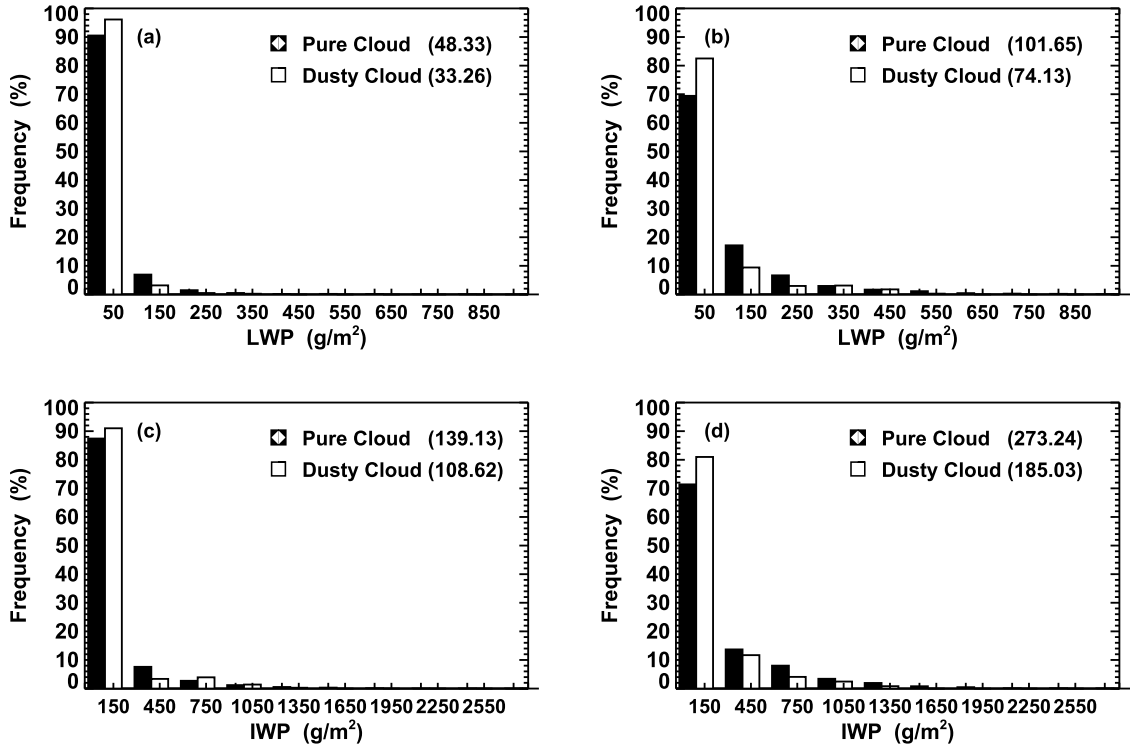

Figure 6. Same as Figure 4 but for the liquid water path (LWP) and ice water path (IWP). Histogram intervals are 100 g m^{-2} for LWP and 300 g m^{-2} for IWP.

compared to 51.7 μm for dusty clouds, a decrease of 6.5%. For both ice and water clouds, smaller particle sizes are more frequent for dusty clouds. Few large particles occur for dusty clouds in the source region.

[18] LWP and IWP are computed from the cloud OPDs and effective particle sizes. The resulting mean values of LWP and IWP for dusty clouds are considerably smaller than those for pure clouds (Figure 6). The average LWP decreases from 48.3 g m^{-2} for pure clouds to 33.3 g m^{-2} for dusty clouds in the source region (Figure 6a) and decreases from 101.7 to 74.1 g m^{-2} in the downwind region for pure and dusty clouds, respectively (Figure 6b). Similar drops are seen in the IWP means. In the source region (Figure 6c) the mean IWP decreases from 139.1 g m^{-2} (pure clouds) to 108.6 g m^{-2} (dusty clouds), while in the downwind region (Figure 6d) it decreases considerably, from 273.2 to 185.0 g m^{-2}. As expected, smaller values of LWP and IWP occur more frequently in dusty clouds than in pure clouds.

[19] To determine if the differences between dusty and pure clouds are statistically significant, we apply the *t*-test for dusty and pure clouds in the source and downwind regions. Because some of the samples are not normally distributed (OPD, LWP, and IWP), we first adjust the samples to obtain a more normal distribution. The widely used method is logarithmic change represented by the equation

$$B_i = \ln A_i \ (i = 1, 2, 3, \ldots, n).$$

[20] After adjustment, the distribution of samples is normal, permitting the use of the *t*-test for statistical significance testing. Since the variances of the dusty and pure cloud samples are not equal, the equation for the *t*-test used here is

$$T = \frac{\bar{x} - \bar{y}}{\sqrt{(V_x/M) + (V_y/N)}},$$

where $\bar{x}$ is the mean value for pure clouds, $\bar{y}$ is the mean value for dusty clouds, V_x is the variance for pure clouds, V_y

Table 2. Significance Test of Differences Between Dusty and Pure Clouds in the Source Region[a]

Property	Mean(Pure) – Mean(Dusty)	Result of *t*-Test	$t(\alpha = 0.05)$	$t(\alpha = 0.01)$
OPD				
Water clouds	1.13	2.21	1.96	2.58
Ice clouds	0.19	1.63	1.96	2.58
LWP (g m^{-2})	15.07	7.07	1.96	2.58
IWP (g m^{-2})	30.51	4.94	1.96	2.58
R_e (μm)	2.35	11.77	1.96	2.58
D_e (μm)	8.3	10.15	1.96	2.58

[a] D_e, effective diameter; IWP, ice water path; LWP, liquid water path; OPD, optical depth; R_e, effective radius.

Table 3. Same as Table 2, but in the Downwind Region[a]

Property	Mean(Pure) – Mean(Dusty)	Result of *t*-test	$t(\alpha = 0.05)$	$t(\alpha = 0.01)$
OPD				
Water clouds	1.13	2.21	1.96	2.58
Ice clouds	4.65	4.79	1.96	2.58
LWP (g m^{-2})	27.52	6.18	1.96	2.58
IWP (g m^{-2})	88.21	4.75	1.96	2.58
R_e (μm)	0.20	1.18	1.96	2.58
D_e (μm)	3.63	3.29	1.96	2.58

[a] D_e, effective diameter; IWP, ice water path; LWP, liquid water path; OPD, optical depth; R_e, effective radius.

is the variance for dusty clouds, M is the number of pure cloud samples, and N is the number of dusty cloud samples.

[21] Table 2 lists the statistical significance of the differences between dusty and pure clouds in the source region. Although there are only 20 cases for each type, the total number of samples for statistical significance is based on individual pixels and the total number of dusty and pure cloud pixels is, at a minimum, greater than 1000, so the number of samples is sufficient for applying the test. If the value of the t parameter is greater than $t(\alpha = 0.05)$ or $t(\alpha = 0.01)$, the differences between dusty and pure clouds are significant at the 95% or 99% level, respectively. The results in Table 2 reveal that the differences between dusty and pure clouds are all significant at the 95% significance level, except for the ice cloud OPD. The values of the t parameter for water clouds are generally larger than those for ice clouds. Table 3 lists the statistical significance of the differences between dusty and pure cloud properties in the downwind region, where the differences between dusty and pure clouds are all significant at the 99% level, except for R_e.

[22] The frequency distributions of mean T_e values for dusty and pure clouds in the source and downwind regions are shown in Figure 7. The temperatures for dusty clouds in both regions are similar to, but slightly higher than, those for pure clouds. In Figures 7a–7d, colder values of T_e are more frequent for pure clouds, suggesting that they sometimes occur in different types of air masses than their dusty counterparts. Assuming a nominal lapse rate of 6.5 K/km and the same air mass for each region, the differences in mean T_e theoretically would translate to Z_e differences of 0.15 and 0.71 km between pure and dusty water clouds in the source and downwind regions, respectively. Similarly, Z_e differences of 0.56 and 1.32 km between pure and dusty ice clouds would be expected in the source and downwind regions, respectively, based on the differences in T_e in Figure 7.

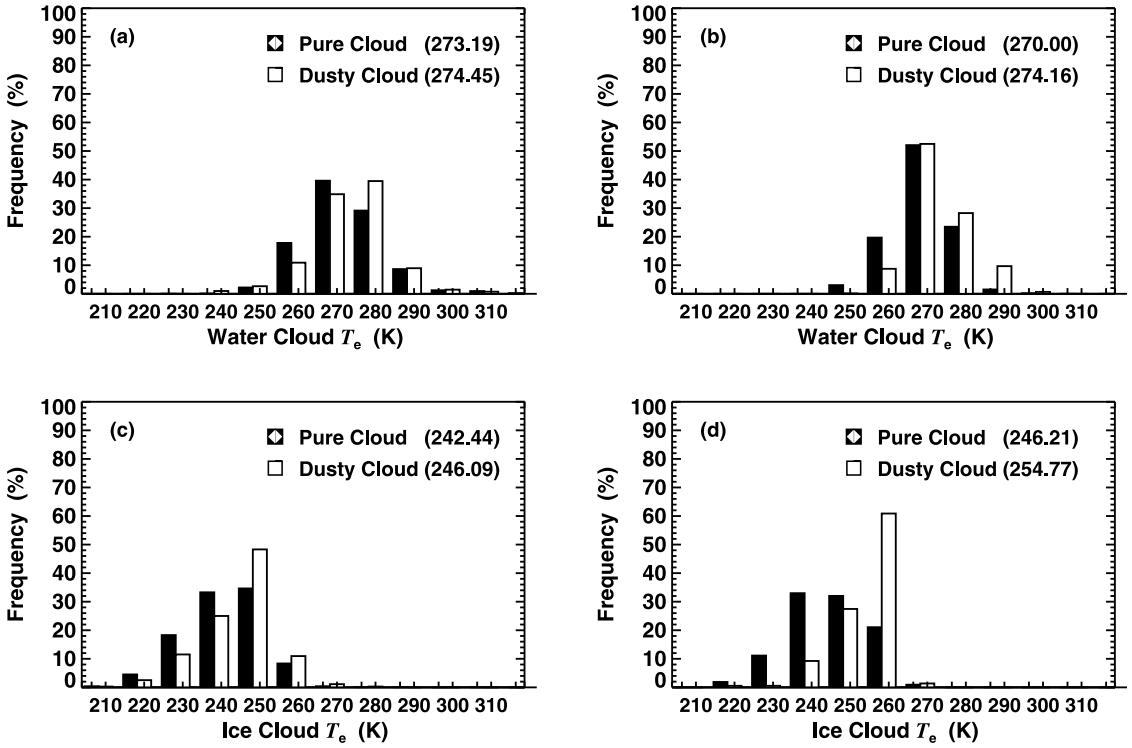

Figure 7. Same as Figure 4, but for cloud effective temperature (T_e). Histogram intervals are 10 K for both water and ice clouds.

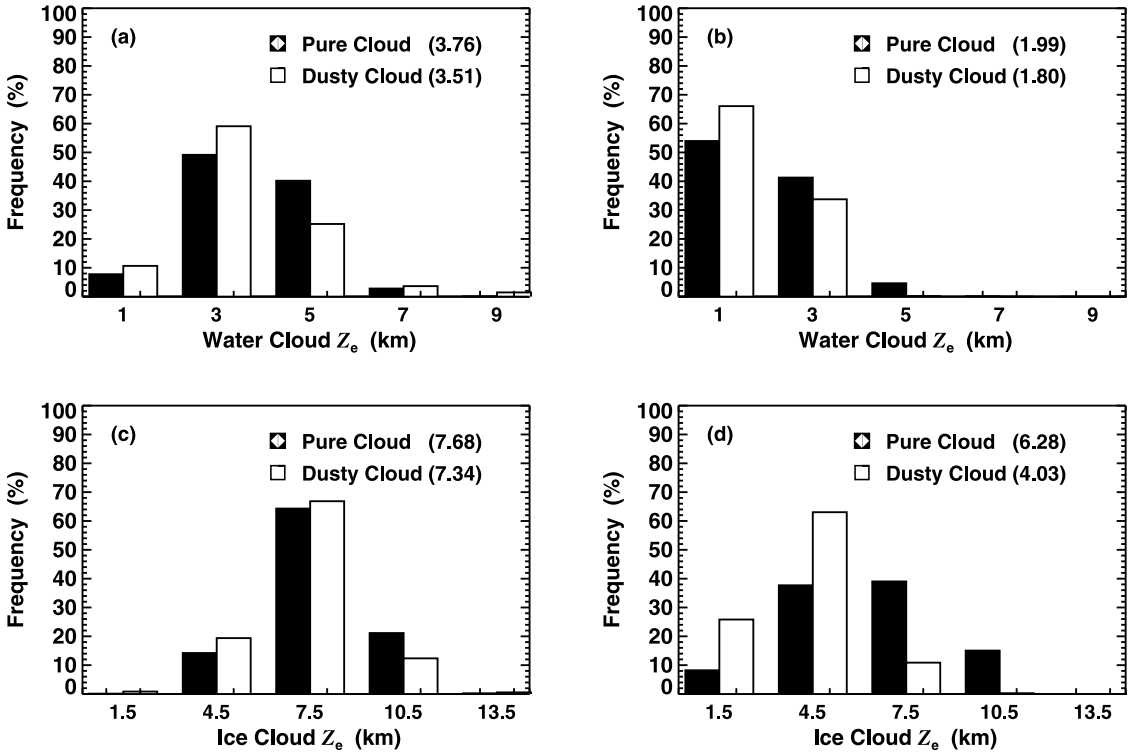

Figure 8. Same as Figure 4, but for cloud effective height (Z_e). Histogram intervals are 2 km for water clouds and 3 km for ice clouds.

[23] Cloud Z_e distributions are plotted in Figure 8. For water clouds the difference in Z_e between dusty and pure clouds is 0.25 km in the source region (Figure 8a) and 0.19 km in the downwind region (Figure 8b). Since there is little difference between the retrieved mean Z_e (Figure 8) and that based on T_e for an assumed common air mass, the "theoretical" Z_e difference, for water clouds in the source region, it is likely that the thermal structure of the lower troposphere was similar for both the dusty and the pure clouds. For the downwind regions the differences suggest that dusty clouds formed in a warmer boundary layer than pure clouds. For ice clouds the difference in Z_e between dusty and pure clouds is 0.34 km in the source region (Figure 8c) and 2.25 km in the downwind region (Figure 8d). Over the source region the Z_e differences between pure and dusty ice clouds can essentially be explained by the moisture occurring at a slightly higher altitude for the pure cloud cases because the theoretical and retrieved Z_e differences differ by only 0.2 km. Thus, in the source region there are apparently no significant differences in the mean thermal structure of the upper troposphere. However, over the downwind region the discrepancy between the retrieved and the theoretical Z_e differences is nearly 1 km, indicating that the upper troposphere is significantly warmer for the dusty cloud cases. Additionally, the height matching was only to within ±1 km, so it is possible that the selected downwind dusty clouds tended to be lower by as much as 1 km in the selection process. This is consistent with the warmer clouds seen in the dusty cases.

[24] Another factor that could contribute to the discrepancy is the differences in ice water content between the downwind dusty and the downwind pure ice clouds. The quantity Z_e is the radiating center of the cloud. It is at a distance downward from the cloud top corresponding to an optical depth of ~1.2, equivalent, on average, to ~2.1 km for optically thick ice clouds [*Minnis et al.*, 2008b]. Because of variations among clouds, however, the depth of Z_e below cloud top ranges up to 6 km or greater depending on the ice water content above the radiating center. This would imply that, since the Z_e for dusty ice clouds is systematically lower than that for pure ice clouds, the ice water contents in the tops of the downwind dusty ice clouds are substantially lower than those for pure clouds. This factor, together with the differences in the thermal structure of the atmosphere and the selection process, could account for the downwind ice cloud height differences.

4.2. Cloud Radiative Forcing

[25] Cloud RF, denoted by the variable C, is defined as the difference between the clear-sky and the total-scene radiation results [*Ramanathan et al.*, 1989]:

$$C_{\mathrm{SW}} = F_{\mathrm{clr}}^{\mathrm{SW}} - F_{\mathrm{SW}},$$

$$C_{\mathrm{LW}} = F_{\mathrm{clr}}^{\mathrm{LW}} - F_{\mathrm{LW}},$$

$$C_{\mathrm{net}} = C_{\mathrm{SW}} + C_{\mathrm{LW}},$$

where $F_{\mathrm{clr}}^{\mathrm{SW}}$ and $F_{\mathrm{clr}}^{\mathrm{LW}}$ are the CERES clear-sky broadband SW and LW radiative fluxes at the TOA, respectively, and F_{SW} and F_{LW} are SW and LW radiative fluxes at the TOA for all sky conditions, clouds and no clouds together. The instantaneous TOA net RF, C_{net}, for pure and dusty clouds in the source and downwind regions is shown in Figure 9

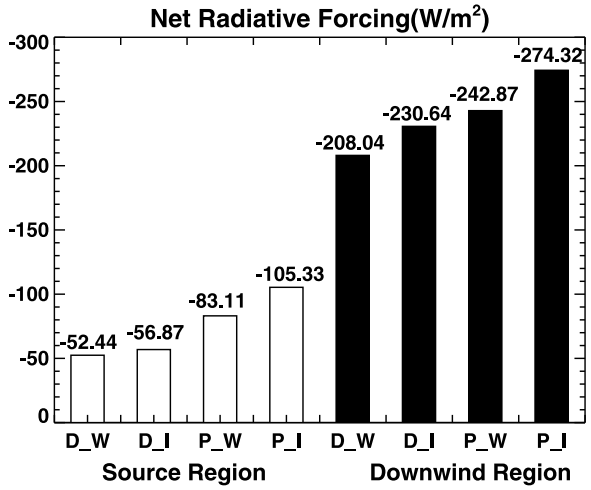

Figure 9. Top-of-atmosphere (TOA) net radiative forcing of dusty (D_I) and pure (P_I) ice clouds and dusty (D_W) and pure (P_W) water clouds in the source and downwind regions.

for various cloud conditions. For water clouds the mean absolute value of instantaneous C_{net} for dusty clouds (D_W) is 52.4 W m^{-2}, which is 36.9% smaller than for pure clouds (P_W) in the source region. In the downwind region the absolute value of C_{net} for dusty clouds (D_W) is 208.0 W m^{-2}, which is 14.3% smaller than for pure clouds (P_W). For ice clouds the absolute value of C_{net} for dusty clouds (D_I) is 56.9 W m^{-2} in the source region, a value ~46.0% smaller than that for pure clouds (P_I). In the downwind region the absolute value of instantaneous C_{net} for dusty clouds (D_I) is 230.6 W m^{-2}, 15.9% smaller than for pure clouds (P_I). Despite the uncertainties in the SW and LW fluxes,these results are considerably accurate and acceptable.

5. Discussion

5.1. Cloud Properties

[26] The results clearly show that, relative to pure clouds, dusty clouds contain less water and have smaller particle sizes and optical depths. These differences could arise for several reasons, with differences in CCN and available humidity being the most dominant because they are the parameters mainly responsible for particle size and water content, respectively. In the dusty regions the aerosols can reduce the size of cloud particles by increasing the number of available CCN. Increased numbers of CCN distribute water vapor among more dust particles, thus reducing the R_e of the cloud droplets for a given supersaturation [*Han et al.*, 2008]. Differences in humidity could cause disparities in OPD, cloud fraction, and R_e. For the same CCN and vertical velocity, a thicker saturated layer would produce a larger OPD, particle size, and water path for liquid clouds because thicker clouds allow for more droplet growth as an air parcel rises through the cloud. Larger droplets eventually lead to collision and coalescence, resulting in even greater droplet sizes. Similarly, a thicker or more saturated ice cloud layer would yield a greater OPD, and the D_e would be larger because it would sublimate more slowly as it falls. A more horizontally extensive saturated layer would likely generate a greater cloud fraction in either case.

Table 4. Mean Relative Humidities 50 hPa Above the Cloud Top and 50 hPa Below the Cloud Base

Source Region (%)				Downwind Region (%)			
Dusty Cloud		Pure Cloud		Dusty Cloud		Pure Cloud	
Below	Above	Below	Above	Below	Above	Below	Above
48.3	49.6	55.2	60.3	61.2	51.1	62.1	55.8

[27] To examine the humidity impact, the mean relative humidity was computed from the NCEP analyses for 50 hPa layers above the cloud top and 50 hPa layers below the cloud base. Additionally, the mean column relative humidity was computed for the same cases including both the sampled and the immediately surrounding 1° boxes. In the source region the relative humidity 50 -hPa above the dusty cloud top is 49.6%, which is 17.7% less than for pure clouds, but below the dusty cloud bases the relative humidity is only 12.5% less than for pure clouds (Table 4). These results suggest that, in the source regions, the moist layers are thicker for pure clouds than for dusty clouds. Generally speaking, a thicker moist layer implies a greater OPD for pure clouds, suggesting that at least some of the differences in cloud fraction, OPD, and LWP are due to the availability of more water vapor for pure clouds in the source regions. However, if the column relative humidity (Table 5) is used as the metric, the humidity seems to play a very minor role in the differences both at the source and downwind.

[28] Downwind, the column relative humidities are ~50% higher than those in the source region. This is not surprising given the geographical differences. Unlike that for the source region, the mean relative humidities immediately above and below the cloud layers (Table 4) differ little between the dusty and the pure cloud cases, especially for water clouds. Thus, in the downwind regions the humidity appears to be an even smaller factor in accounting for the cloud microphysical property differences than in the source region. However, the differences in the cloud microphysical properties are not very large either. As discussed in section 4.1, the thermal structure of the troposphere is likely to be different, warmer overall, for the dusty cloud cases than for pure clouds. This variance could cause differences in the formation mechanisms that affect the microphysical properties. Analyzing that effect would require detailed model analyses and is beyond the scope of this study.

[29] Isolating the effect on cloud properties owing purely to increases in CCN implied from the differences between

Table 5. Mean Relative Humidity of Dusty and Pure Cloud in the Source and Downwind Regions

Region	Percentage
Source	
Dusty cloud	50.95
Pure cloud	50.78
Downwind	
Dusty cloud	74.94
Pure cloud	74.56

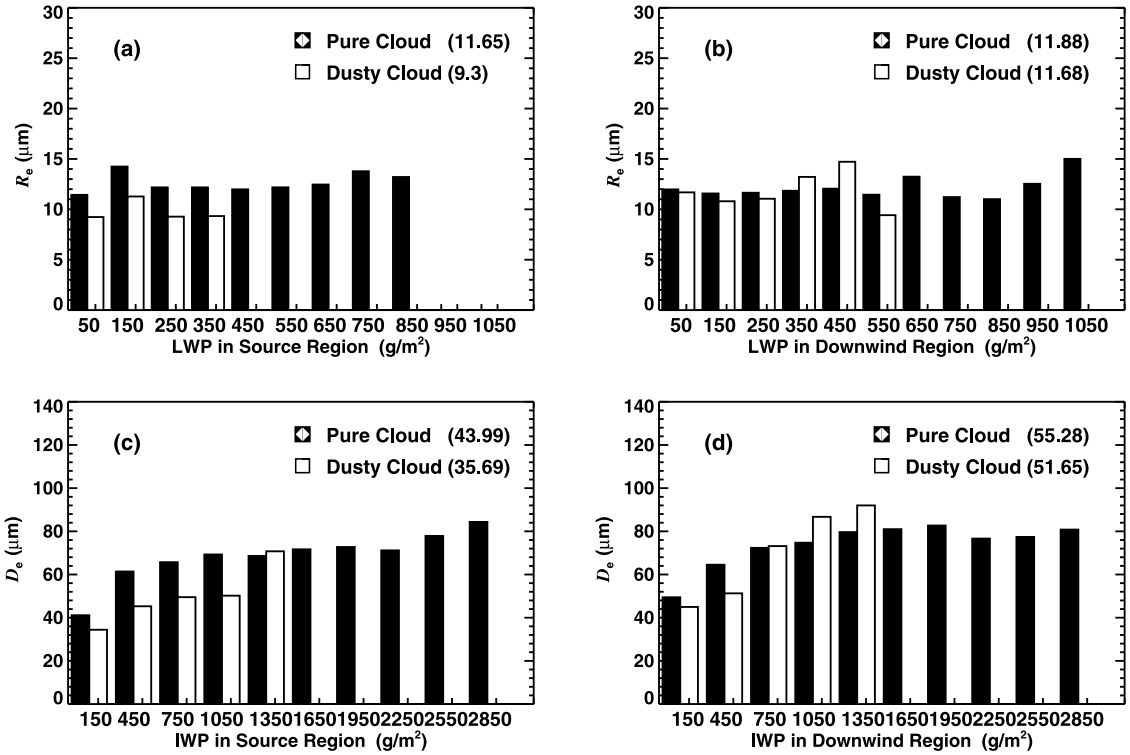

Figure 10. Comparison of (a, b) R_e and (c, d) D_e as a function of liquid water path (LWP) and ice water path (IWP) between dusty and pure clouds over (a, c) the source and (b, d) the downwind regions.

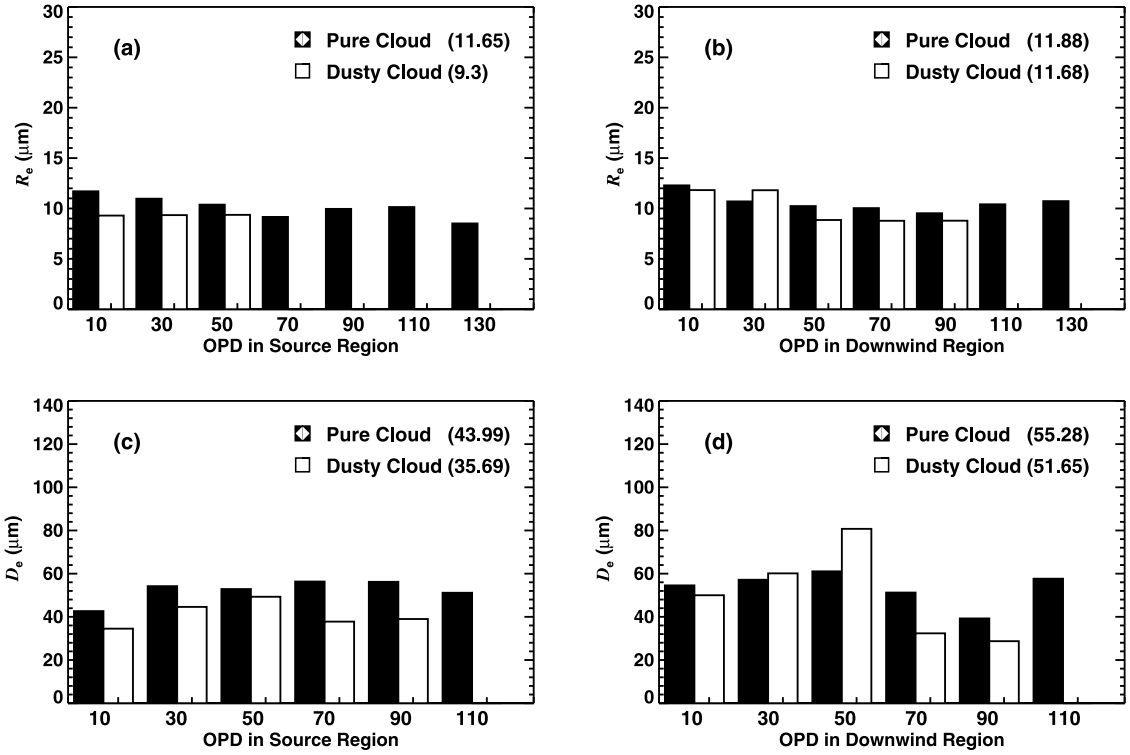

Figure 11. Comparison of (a, b) R_e and (c, d) D_e as a function of water and ice cloud OPDs between dusty and pure clouds over (a, c) the source and (b, d) the downwind regions.

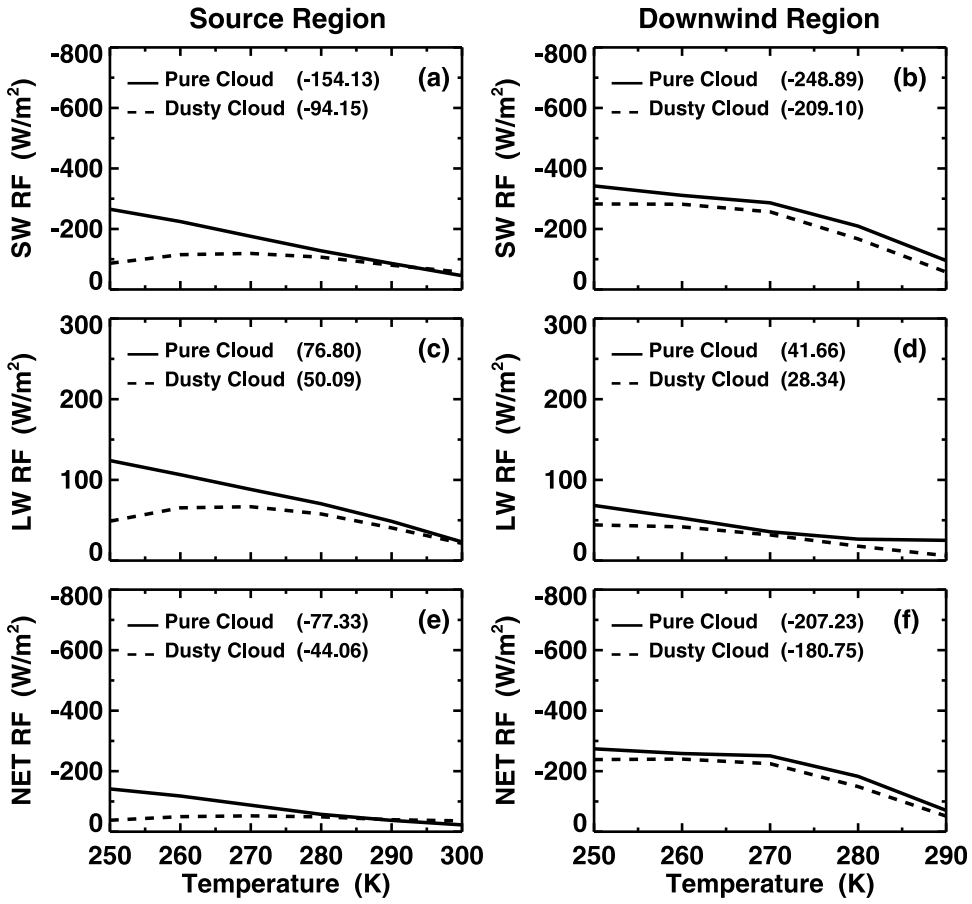

Figure 12. Comparison of TOA short-wave (SW), long-wave (LW), and net radiative forcing (RF) as a function of T_e for water clouds between (a, c, e) the source and (b, d, f) the downwind regions.

the dusty and the pure cloud regions is difficult, but it is most closely obtained for particle size by examining R_e and D_e for the same values of water path and optical depth. A given value of cloud LWP or IWP presumably represents all of the water vapor available for condensation in a cloud so that humidity is not a factor and differences in particle size are primarily due to CCN or IN abundance. Figures 10 and 11 show the distributions of particle size as functions of water path and OPD, respectively. In the source regions, it is clear that both R_e (Figures 10a and 11a) and D_e (Figures 10c and 11c) for dusty clouds are significantly lower than for their pure cloud counterparts in all water path and OPD intervals, except for IWP > 1200 g m^{-2}. That exception represents very few samples. In the downwind regions the dusty cloud R_e is smaller for all intervals having LWP < 300 g m^{-2} (Figure 10b) and OPD < 20 (Figure 11b), but only by ~1.5 μm. It is much larger for thicker clouds, but those clouds constitute a negligible part of the entire data set. Similarly, D_e for the dusty clouds is smaller for IWP < 600 g m^{-2} (Figure 10d) and OPD < 20 (Figure 11d). Again, these pixels account for most of the ice cloud cases. These results are strong evidence that the particle size differences between dusty and pure clouds are mostly the result of the dust aerosols, not the humidity in the source region. However, the particle size difference between dusty and pure clouds is not as evident in the downwind region.

[30] The stronger impact of the dust in the source region is reasonable given that the dust loading should be greater there than downwind. A number of factors likely cause the R_e similarities between dusty and pure clouds in the downwind region. At low levels the dust loading in the downwind region is 4–5 times lower than over the source regions [*Huang et al.*, 2008], probably due to fallout or washout of the dust at low levels by the time the air reaches the coast. The finer dust aloft in the source region is carried much farther and higher by strong winds and, therefore, would affect the high clouds but not the low clouds. This may be reflected by the greater decrease in D_e downwind. At low levels the downwind region is heavily polluted with a variety of aerosols from anthropogenic sources, and there is greater humidity and more hydrophilic material in the downwind region. The presence of those aerosols would diminish the susceptibility of the clouds to further changes in the cloud microphysical properties. The dust effects would probably be different for a downwind area having a more pristine boundary layer.

[31] As noted earlier, the humidity differences could account, at least in part, for the slightly larger OPD of the liquid water cloud OPD and could affect the particle size because thicker clouds allow for more growth of a droplet as an air parcel rises through the cloud. However, since the mean ice cloud OPDs in the source region are nearly iden-

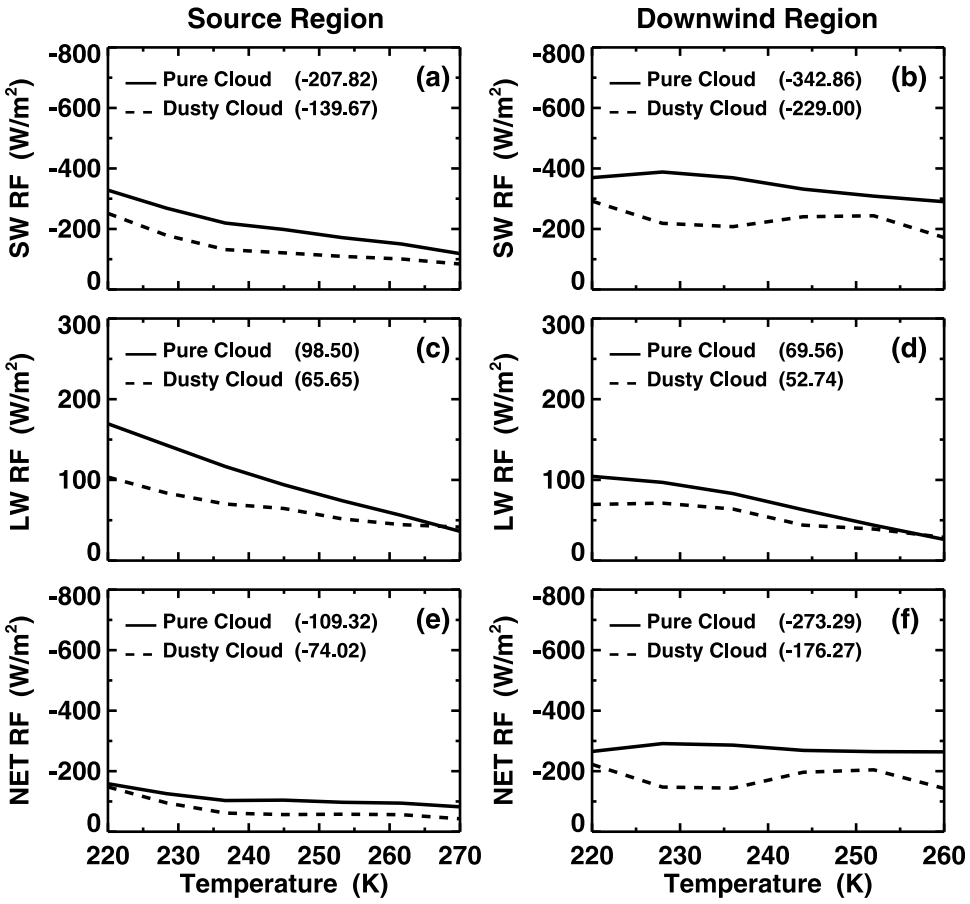

Figure 13. Same as Figure 12, but for ice clouds.

tical, despite the differences in humidity above and below the clouds (Table 4), it is concluded that the differences in D_e and IWP are primarily due to the dust aerosol increasing the IN concentrations in the dusty clouds. Given the pure versus dusty differences in the downwind ice cloud temperatures noted earlier, it is possible that the small (~7%) decrease in D_e actually underestimates the dust impact because D_e typically increases with increasing cloud temperature [e.g., *Heymsfield and Platt*, 1984]. Thus, with all other parameters being the same for a given OPD, the D_e in the dusty clouds over the downwind region should be larger than its pure counterpart because T_e is 8.6 K greater in the dusty clouds. Nevertheless, the downwind D_e difference in the ice clouds is still somewhat consistent with PACDEX aircraft observations far downwind of the source regions. *Stith et al.* [2009] found that the dust plumes had only a small impact on total CCN concentrations but exhibited high concentrations of IN.

[32] As mentioned earlier, differences in humidity can probably account for some of the differences between the dusty and the pure cloud fractions, but how much is difficult to assess without an in-depth modeling study. Another potential explanation for the differences in the cloud fractions could be the heating effect of dust aerosols. Absorption of radiation by dust particles may evaporate cloud droplets, thus diminishing the cloud fraction, so the cloud fraction for dusty clouds is less than that for pure clouds. This would constitute the dust aerosols' semidirect effect. These and other potential sources of cloud property differences will require a greater number of cases combined with some cloud modeling analyses.

5.2. Radiative Forcing

[33] The results in Figure 9 demonstrate that the net cloud RF is possibly reduced by dust aerosols at the TOA in the source region and that the dust aerosols also inhibit the cooling effect of clouds. In the downwind region the net cloud RF may also be reduced by dust aerosols, while for the 20 cases, there are also many other factors. In addition, the absolute values of C_{net} for dusty and pure clouds (both water and ice clouds) in the downwind region are both larger than in the source region. This is because RF at the TOA not only is affected by the spatial distribution of clouds, but also depends on other factors, including surface albedo, optical properties of the aerosols and clouds, and available moisture. Because the surface albedo in the Pacific Region (6%–8%) is less than that in the continental region (25%–35%), the largest negative RF values often appear over the ocean. The smaller optical depths of dusty clouds would cause slightly less SW forcing than those of pure clouds.

[34] The instantaneous SW RF, LW RF, and net RF are shown as functions of T_e in the source and downwind regions for water and ice clouds in Figures 12 and 13, respectively. For both water and ice clouds the absolute

values of RF (SW, net, and LW) decrease with increasing T_e, and the mean absolute values of RF (SW, LW, and net) for dusty clouds are less than those of pure clouds in both the source and the downwind regions. This behavior is not surprising, owing to the effect of dust aerosols on cloud and radiative properties and other factors already mentioned. In addition, the difference in humidity in the source and downwind regions will affect the LW RF. As in the case of the microphysical properties, completely isolating the effect of the dust on the cloud RF will require a combination of measurements like those reported here and detailed cloud and radiative transfer modeling.

6. Conclusions

[35] Mineral dust aerosols are an important component of the Earth's climate system, possibly acting to accelerate the aridification of northern China. Dust generated in the Taklamakan and Gobi deserts and Asian pollution can become entrained and transported by westerly jets across eastern Asia and the Pacific Ocean, and may even reach North America. Dust plumes often pass through Pacific Ocean extratropical cloud systems, which are important climate regulators owing to their large radiative cooling effect. The effect of this mixed dust-pollution plume on Pacific cloud systems and their associated RF is an unexplored, yet key factor for understanding climate change. In this article the case studies and statistical analyses document different dust effects on clouds over the source and downwind regions during the PACDEX period (March through May 2007), a season that is typically active for dust event development. The geographical locations of these study areas represent the upstream portion of the PACDEX regions of interest.

[36] In this study the results show that the impact of dust aerosols on cloud properties and RF is very complex. Dust aerosols change the microphysical characteristics of the clouds, reducing the cloud effective particle size and, possibly, OPD, LWP, and IWP, especially in the source region. This implies that dust aerosols might be an important factor in suppression of precipitation by reducing the opportunity for the development of the larger hydrometeors necessary for precipitation. Once these aerosols enter the cloud in a dust storm or dust devil, they will participate in the cloud physical processes as CCN, thus greatly increasing the CCN concentrations by distributing water vapor between more dust particles, reducing the R_e of cloud droplets, and suppressing the occurrence of precipitation. However, the decreased cloud OPD and water path reduce the cloud cooling effect, in essence, causing an increased warming effect. The comparison of OPD, R_e/D_e, and LWP/IWP differences between dusty and pure clouds in the source and downwind regions confirms that the dust aerosol impacts are greater in the source region than in the downwind region. In addition, for water clouds the absolute value of instantaneous net RF for pure clouds is reduced by 36.9% and 14.3% in the source and downwind regions, respectively. For ice clouds the absolute value of instantaneous net RF for pure clouds is reduced by 46.0% and 15.9% in the source and downwind regions, respectively. Although there are only 20 cases for each classification, the statistical significance results are based on pixel-level calculations and the total numbers of dusty and pure cloud pixels are at least larger than 1000, so differences are statistically significant, and they are consistent with previous conclusions [*Huang et al.*, 2006a, 2006b]. In addition, cloud lifetime and formation mechanisms are all parameters that can affect cloud microphysics but cannot be determined without a detailed modeling study that is beyond the scope of this article. In the future we need more cases to test the conclusions of this study in more aspects.

[37] Another possible mechanism of dust impact on climate is through the semidirect effect, which is related to the absorption of solar radiation by dust aerosols [*Huang et al.*, 2006b]. The absorption or diabatic heating of Asian dust can cause the evaporation of cloud droplets and reduce the cloud water path. Owing to the large spatial and temporal extent of desert dust in the atmosphere, the interactions of desert dust with clouds can have substantial climatic impacts. The decreasing cloud OPD and water path partially reduce the cloud cooling thus increasing the warming. It has been commonly believed that the desert dust might contribute significantly to the observed reductions in cloud droplet size and precipitation over Africa [*Rosenfeld et al.*, 2001]. However, the semidirect effect may be dominated by dust aerosol-cloud interaction over arid and semiarid areas in East Asia and contribute to reduced precipitation via a mechanism significantly different from that in Africa. Dust aerosols may have contributed to the desertification of northwestern China during recent decades [*Huang et al.*, 2006b].

[38] This study also demonstrated that dust aerosol effects on ice clouds could be greater than those on water clouds in the downwind region. For example, there was a negligible difference between the dusty and the pure cloud R_e in the downwind region, while the D_e was smaller by 7%, even though it probably should have been larger because the dusty ice clouds were significantly warmer than the pure clouds. The downwind results are consistent with PACDEX aircraft observations, which demonstrated that dust aerosols should have a larger effect on ice clouds than on water clouds in the downwind region. IN concentrations in downwind dust plumes exceeded typical tropospheric values by 4 to 20 times and were similar to those in previous studies of the Saharan aerosol layer [*Stith et al.*, 2009]. Enhanced IN concentrations were found in the upper troposphere off the coast of North America, providing the first direct validation of the transport of dust layers containing high IN concentrations near the tropopause entering the North American continent from distant sources [*Stith et al.*, 2009].

[39] Although this study indicates that the dust effects on cloud properties are less in the downwind region than in the source region, the impact of long-range transport of dust and air pollution from their continental sources over the oceanic regions is, however, one of the outstanding problems in regional and global climate change. Dust mixed with air pollution leads to a brownish haze, which absorbs and scatters sunlight and leads to a large reduction in sunlight at the surface [*Ramanathan et al.*, 2001], resulting in so-called "global dimming." The vertical structure and degree of vertical mixing between dust and pollution layers as they are transported are, however, poorly known. The widespread dust and pollution over the northern Pacific Ocean makes it one of the largest pollution-affected oceanic re-

gions of the world, at least during springtime. This transport is quite efficient, sometimes moving the hazy mixture across the Pacific from Asia to North America. Because of the fast large-scale transport in the upper troposphere, once aerosols, such as dust and black carbon, enter the upper troposphere (above 8 km), they can be transported around the Earth in a latitudinal belt within 1 to 2 weeks [*Huang et al.*, 2008]. As a result, dust from Asia can impact upper tropospheric clouds over North America and the Atlantic as well. For example, *DeMott et al.* [2003] found that fine dust from North Africa contributed significantly to ice nuclei populations over Florida. Using ground-based lidar polarization data, *Sassen* [2002] found that Asian dust affected the formation and phase of ice clouds over the western United States, leading to unusually warm cirrus clouds. Several studies have reported that dust aerosols generated in the Taklamakan and Gobi areas can be transported eastward by prevailing westerlies over China, North and South Korea, and Japan [*Iwasaka et al.*, 1983; *Zhang et al.*, 1997; *Murayama et al.*, 2001; *Uno et al.*, 2001; *Natsagdorj et al.*, 2003; *Huang et al.*, 2008] and are carried even farther across the Pacific Ocean, reaching North America [*Husar et al.*, 2001; *Uno et al.*, 2001; *Sassen*, 2002]. Asian dust effects on the downwind region's cloud and radiative properties still need to be explored in more detail.

[40] The conclusions from this study are based only on satellite data taken during the PACDEX (March–May 2007) field experiment period and do not cover a sufficient time span to definitively quantify the observed dust effect on clouds over the two regions. Long-term monitoring and detailed analysis are necessary to determine the full scope and statistical significance of these effects. Since dust's direct radiative effects are important in modulating the global and regional climate, further research should focus on combining A-Train satellite measurements with PACDEX aircraft and surface site measurements.

[41] **Acknowledgments.** This research was supported by the National Science Foundation of China under grants 40725015 and 40633017, by the Knowledge Innovation Program of the Chinese Academy of Sciences under grant IAP09311, by the NASA Science Mission through the CALIPSO Project, and by the Radiation Sciences Program through the CERES Project. The CALIPSO, CERES Single Scanner Footprint, and CloudSat data were obtained from the NASA Earth Observing System Data and Information System, Atmospheric Sciences Data Center (ASDC), at Langley Research Center.

References

Chen, L., Y. Yin, J. Yang, and S. Niu (2007), Effects of sand dust particles on cloud and precipitation: A numerical study, *J. Nanjing Inst. Meteorol.* (in Chinese), *30*(5), 590–600.

Chiriaco, M., et al. (2007), Comparison of CALIPSO-like, LaRC, and MODIS retrievals of ice cloud properties over SIRTA in France and Florida during CRYSTAL-FACE, *J. Appl. Meteorol. Climatol.*, *46*, 249–272.

Collins, W. D., W. C. Conant, and V. Ramanathan (1994), Earth radiation budget, clouds and climate sensitivity, in *The Chemistry of the Atmosphere: Its Impact on Global Change*, edited by J. G. Calvert, pp. 207–215, Blackwell Scientific, Oxford.

DeMott, P. J., K. Sassen, M. R. Poellot, D. Baumgardner, D. C. Rogers, S. D. Brooks, A. J. Prenni, and S. M. Kreidenweis (2003), African dust aerosols as atmospheric ice nuclei, *Geophys. Res. Lett.*, *30*(14), 1732, doi:10.1029/2003GL017410.

Dong, X., P. Minnis, B. Xi, S. Sun-Mack, and Y. Chen (2008), Comparision of CERES-MODIS stratus cloud properties with ground-based measurements at the DOE ARM Southern Great Plains site, *J. Geophys. Res.*, *113*, D03204, doi:10.1029/2007JD008438.

Han, Y., Y. Chen, X. Fang, and T. Zhao (2008), The possible effect of aerosol on precipitation in Trim basin, *China Environ. Sci.* (in Chinese), *28*(2), 102–106.

Heymsfield, A. J., and C. M. R. Platt (1984), A parameterization of the particle size spectrum of ice clouds in terms of ambient temperature and ice water content, *J. Atmos. Sci.*, *41*, 846–855.

Hu, Y., Z. Liu, D. Winker, M. Vaughan, V. Noel, L. Bissonnette, G. Roy, and M. McGill (2006), A simple relation between lidar multiple scattering and depolarization for water clouds, *Opt. Lett.*, *31*, 1809–1811.

Huang, J., Y. Wang, T. Wang, and Y. Yi (2006a), Dusty cloud radiative forcing derived from satellite data for middle latitude region of East Asia, *Prog. Nat. Sci.*, *10*, 1084–1089.

Huang, J., P. Minnis, B. Lin, T. Wang, Y. Yi, Y. Hu, S. Sun-Mack, and K. Ayers (2006b), Possible influences of Asian dust aerosols on cloud properties and radiative forcing observed from MODIS and CERES, *Geophys. Res. Lett.*, *33*, L06824, doi:10.1029/2005GL024724.

Huang, J., P. Minnis, Y. Yi, Q. Tang, X. Wang, Y. Hu, Z. Liu, K. Ayers, C. Trepte, and D. Winker (2007), Summer dust aerosols detected from the CALIPSO satellite over the Tibetan Plateau, *Geophys. Res. Lett.*, *34*, L18805, doi:10.1029/2007GL029938.

Huang, J., P. Minnis, B. Chen, Z. Huang, Z. Liu, Q. Zhao, Y. Yi, and K. Ayers (2008), Long-range transport and vertical structure of Asian dust from CALIPSO and surface measurements during PACDEX, *J. Geophys. Res.*, *113*, D23212, doi:10.1029/2008JD010620.

Husar, R. B., et al. (2001), Asian dust events of April 1998, *J. Geophys. Res.*, *106*, 18317–18330.

Iwasaka, Y., H. Minoura, and K. Nagaya (1983), The transport and spatial scale of Asian dust-storm clouds: A case study of the dust-storm event of April 1979, *Tellus, Ser. B*, *35*, 189–196.

Kalnay, E., et al. (1996), The NCEP/NCAR 40-year reanalysis project, *Bull. Am. Meteorol. Soc.*, *77*, 437–471.

Li, Z. (2004), Aerosol and climate: A perspective from East Asia, in *Observation, Theory, and Modeling of the Atmospheric Variability*, edited by X. Zhu, pp. 501–525, World Scientific, Singapore.

Liu, D., Z. Wang, Z. Liu, D. Winker, and C. Trepte (2008), A height resolved global view of dust aerosols from the first year CALIPSO lidar measurements, *J. Geophys. Res.*, *113*, D16214, doi:10.1029/2007JD009776.

Liu, Z., W. Hunt, M. A. Vaughan, C. A. Hostetler, M. McGill, K. Powell, D. Winker, and Y. Hu (2006), Estimating random errors due to shot noise in backscatter lidar observations, *Appl. Opt.*, *45*, 4437–4447, doi:10.1364/AO.45.004437.

Liu, Z., et al. (2008), CALIPSO lidar observations of optical properties of Saharan dust: A case study of long-range transport, *J. Geophys. Res.*, *113*, D07207, doi:10.1029/2007JD008878.

Loeb, N. G., S. Kato, K. Loukachine, and N. Manalo-Smith (2005), Angular distribution models for top-of-atmosphere radiative flux estimation from the Clouds and Earth's Radiant Energy System instrument on the Terra satellite, Part 1: Methodology, *J. Atmos. Ocean. Technol.*, *22*, 338–351.

Loeb, N. G., S. Kato, K. Loukachine, N. Manalo-Smith, and D. R. Doelling (2007), Angular distribution models for top-of-atmosphere radiative flux estimation from the Clouds and the Earth's Radiant Energy System instrument on the Terra satellite, Part II: Validation, *J. Atmos. Ocean. Technol.*, *24*, 564–584.

Mace, G. G., Y. Zhang, S. Platnick, M. D. King, P. Minnis, and P. Yang (2005), Evaluation of cirrus cloud properties from MODIS radiances using cloud properties derived from ground-based data collected at the ARM SGP site, *J. Appl. Meteorol.*, *44*, 221–240.

Mace, G. G., R. Marchand, Q. Zhang, and G. Stephens (2007), Global hydrometeor occurrence as observed by Cloudsat: Initial observations from Summer 2006, *Geophys. Res. Lett.*, *34*, L09808, doi:10.1029/2006GL029017.

Minnis, P., et al. (2008a), Cloud detection in non-polar regions for CERES using TRMM VIRS and Terra and Aqua MODIS data, *IEEE Trans. Geosci. Remote Sens.*, *46*, 3857–3884.

Minnis, P., C. R. Yost, S. Sun-Mack, and Y. Chen (2008b), Estimating the physical top altitude of optically thick ice clouds from thermal infrared satellite observations using CALIPSO data, *Geophys. Res. Lett.*, *35*, L12801, doi:10.1029/2008GL033947.

Murayama, T., et al. (2001), Ground-based network observation of Asian dust events of April 1998 in east Asia, *J. Geophys. Res.*, *106*(D16), 18345–18360.

Natsagdorj, L., D. Jugder, and Y. Chung (2003), Analysis of dust storms observed in Mongolia during 1937–1999, *Atmos. Environ. 37*, 1401–1411.

Niu, S. (2001), Researches on the distribution of dust aerosols particle spectrum in Helan Mountain area, *Atmos. Sci.*, *25*, 242–252.

Ramanathan, V., et al. (1989), Cloud radiative forcing and climate: Results from the Earth Radiation Budget Experiment, *Science*, *243*, 57–63.

Ramanathan, V., et al. (2001), Indian Ocean experiment: An integrated analysis of the climate forcing and effects of the great Indo-Asian haze, *J. Geophys. Res.*, *106*(D22), 28371–28398.

Ramaswamy, V., O. Boucher, J. Haigh, D. Hauglustaine, J. Haywood, G. Myhre, T. Nakajima, G. Y. Shi, and S. Solomon (2001), Radiative forcing of climate change, in *Climate Change 2001: The Scientific Basis, Contribution of Working Group I to Third Assessment Report of the Intergovernmental Panel on Climate Change*, edited by J. T. Houghton et al., pp. 349–416, Cambridge Univ. Press, New York.

Rosenfeld, D., Y. Rudich, and R. Lahav (2001), Desert dust suppressing precipitation-a possible desertification feedback loop, *Proc. Natl. Acad. Sci. U.S.A.*, *98*, 5975–5980.

Sassen, K. (2002), Indirect climate forcing over the western US from Asian dust storms, *Geophys. Res. Lett.*, *29*(10), 1465, doi:10.1029/2001GL014051.

Smith, W. L., P. Minnis, H. Finney, R. Palikonda, and M. M. Khaiyer (2008), An evaluation of operational GOES-derived single-layer cloud top heights with ARSCL over the ARM Southern Great Plains site, *Geophys. Res. Lett.*, *35*, L13820, doi:10.1029/2008GL034275.

Stephens, G. L., et al. (2002), The CloudSat Mission and the A-Train: A new dimension of space-based observations of clouds and precipitation, *Bull. Am. Meteorol. Soc.*, *83*, 1771–1790.

Stith, J. L., V. Ramanathan, W. A. Cooper, G. Roberts, P. J. DeMott, and G. Carmichael (2009), An overview of aircraft observations from the PACDEX campaign, *J. Geophys. Res.*, *114*, D05207, doi:10.1029/2008JD010924.

Uno, I., H. Amano, S. Emori, K. Kinoshita, I. Matsui, and N. Sugimoto (2001), Trans- Pacific yellow sand transport observed in April 1998: A numerical simulation, *J. Geophys. Res.*, *106*(D16), 18,331–18,344, doi:10.1029/2000JD900748.

Vaughan, M., et al. (2004), Fully automated analysis of space-based lidar data: An overview of the CALIPSO retrieval algorithms and data products, *Proc. SPIE Int. Soc. Opt. Eng.*, *5575*, 16–30.

Waliser, D., et al. (2009), Cloud ice: A climate model challenge with signs and expectations of progress, *J. Geophys. Res.*, *114*, D00A21, doi:10.1029/2008JD010015.

Wielicki, B. A., B. R. Barkstorm, E. F. Harrison, R. B. Lee III, G. L. Smith, and J. E. Cooper (1996), Clouds and the Earth's radiant energy systerm (CERES): An earth observing systerm experiment, *Bull. Am. Meteorol. Soc.*, *77*, 853–868.

Wielicki, B. A., et al. (1998), Clouds and the Earth's Radiant Energy System (CERES): Algorithm overview, *IEEE Trans. Geosci. Remote Sens.*, *36*, 1127–1141.

William, J. R., F. Wu, and D. J. Gaffen (2000), Interannual variability of the tropical tropopause derived from radiosonde data and NCEP reanalyses, *J. Geophys. Res.*, *105*(D12), 15,509–15,523.

Winker, D. M., W. H. Hunt, and M. J. McGill (2007), Initial performance assessment of CALIOP, *Geophys. Res. Lett.*, *34*, L19803, doi:10.1029/2007GL030135.

Yin, Y., and L. Chen (2007), The effects of heating by transported dust layers on cloud and precipitation: A numerical study, *Atmos. Chem. Phys.*, *7*, 3497–3505.

Zhang, X., R. Arimoto, and Z. S. An (1997), Dust emission from Chinese desert sources linked to variations in atmospheric circulation, *J. Geophys. Res.*, *102*(D23), 28,041–28,044.

Zhang, X., et al. (2003), Characterization of soil dust aerosol in China and its transport and distribution during 2001 ACE Asia: Network observations, *J. Geophys. Res.*, *108* (D9), 4261, doi:10.1029/2002JD002632.

Zhou, Z. (2001), Blowing sand and sand storm in China in recently 45 years, *Quat. Sci.* (in Chinese), *21*(1), 9–17.

J. K. Ayers, SSAI, One Enterprise Parkway, Hampton, VA 23666, USA.

Y. Hu and P. Minnis, NASA Langley Research Center, Hampton, VA 23666, USA.

J. Huang, Z. Huang, J. Li, T. Wang, and W. Wang, Key Laboratory for Semi-Arid Climate Change of the Ministry of Education, College of Atmospheric Sciences, Lanzhou University, Lanzhou 730000, P.R. China. (hjp@lzu.edu.cn)